

Localized Calibration: Metrics and Recalibration

Rachel Luo^{*†}, Aadyot Bhatnagar^{*‡}, Huan Wang[‡], Caiming Xiong[‡], Silvio Savarese[†], Yu Bai[‡],
Shengjia Zhao[†], and Stefano Ermon[†]

[†]Stanford University

[‡]Salesforce Research

{rsluo, ssilvio, sjzhao, ermon}@stanford.edu, {abhatnagar, huan.wang,
yu.bai, cxiong}@salesforce.com

Abstract

Probabilistic classifiers output confidence scores along with their predictions, and these confidence scores must be well-calibrated (i.e. reflect the true probability of an event) to be meaningful and useful for downstream tasks. However, existing metrics for measuring calibration are insufficient. Commonly used metrics such as the expected calibration error (ECE) only measure global trends, making them ineffective for measuring the calibration of a particular sample or subgroup. At the other end of the spectrum, a fully individualized calibration error is in general intractable to estimate from finite samples. In this work, we propose the local calibration error (LCE), a fine-grained calibration metric that spans the gap between fully global and fully individualized calibration. The LCE leverages learned features to automatically capture rich subgroups, and it measures the calibration error around each individual example via a similarity function. We then introduce a localized recalibration method, LoRe, that improves the LCE better than existing recalibration methods. Finally, we show that applying our recalibration method improves decision-making on downstream tasks.

1 Introduction

A probabilistic classifier outputs a probability along with each prediction to reflect its confidence in that prediction, and the classifier is *well-calibrated* if these probabilities reflect the true probability of a correct classification. Calibration is an extremely important property in any probabilistic system. Whenever cost-sensitive decision making or model trustworthiness is required, the model should be well-calibrated; applications range from autonomous driving [1, 2] to financial

decision-making [3] to medical diagnosis [4, 5].

Unfortunately, there is currently no interpretable metric for measuring the quality of each probabilistic prediction. Ideally, we want to predict the probability of mis-classification for each individual sample. However, each sample is observed only once for most datasets (e.g. image classification datasets do not contain identical images), making it difficult to infer the mis-classification probability. At the other extreme, commonly used metrics such as the expected calibration error (ECE) measure the probability of mis-classification *averaged* across the entire dataset. Consequently, ECE can be accurately estimated but does not measure the reliability of individual predictions, thus providing little information about the calibration of a particular sample or subgroup.

In this work, we propose local calibration error (LCE), a calibration metric that spans the gap between fully global and fully individualized calibration. We approximate the mis-classification probability of an individual sample by computing the average classification error on similar samples, where similarity is defined by a kernel function in a pretrained feature space. By choosing the number of averaged samples, we can trade-off estimation accuracy and individualization: for a large sample size, we recover the ECE metric; for a small sample size, we recover individual calibration. For an intermediate sample size, our metric can be accurately estimated, and provides some measurement on the reliability of individual predictions.

In addition, we introduce a post-hoc Localized Recalibration method (LoRe), for lowering the LCE. Our method works by learning an additional neural network layer that maps a model’s original confidences to better calibrated confidences. Recalibration with our method improves performance on various downstream applications including calibration of non-class-based

^{*}Equal contribution. Order determined by coin flip.

subgroups (which has implications for fairness) and cost-sensitive decision making.

In summary, the contributions of our paper are as follows.

1. We introduce a local calibration metric, the LCE, that is easier to estimate than a fully individualized calibration error and more useful for measuring calibration within a local neighborhood than a fully global calibration error.
2. We introduce a post-hoc localized recalibration method LoRe, that transforms a model’s confidence predictions to improve the local calibration.
3. We empirically evaluate the performance on several downstream tasks after recalibration with our method, and show that our method outperforms existing global recalibration methods on these downstream tasks.

2 Background and Related Work

2.1 Calibration

A classification task maps from some input domain (e.g. images) \mathcal{X} to a finite set of labels $\mathcal{Y} = \{1, \dots, m\}$. A classifier is a pair (f, \hat{p}) where $f : \mathcal{X} \rightarrow \mathcal{Y}$ maps each input $x \in \mathcal{X}$ to a label $y \in \mathcal{Y}$ and $\hat{p} : \mathcal{X} \rightarrow [0, 1]$ maps each input x to a confidence value c . The classifier (f, \hat{p}) is perfectly calibrated [6, 7, 8, 9] with respect to the joint distribution P^* on $\mathcal{X} \times \mathcal{Y}$ if $\forall c \in [0, 1]$

$$\Pr_{P^*(X,Y)} [f(X) = Y \mid \hat{p}(X) = c] = c. \quad (1)$$

To numerically measure how well a classifier is calibrated, the most commonly used metric is Expected Calibration Error (ECE) [10] defined by

$$\text{ECE}(f, \hat{p}) := \mathbb{E}_{X,Y} \left[\left| \hat{p}(X) - \mathbb{E}[f(X) = Y \mid \hat{p}(X)] \right| \right] \quad (2)$$

In other words, ECE measures the average deviation from Eq. 1. In practice, the ECE is approximated by binning — partitioning the predicted confidences into bins, and then taking the sample-weighted average of the difference between the average confidence and average accuracy for each bin.

2.2 Existing Global Recalibration Methods

Many existing methods apply a post-hoc adjustment that changes a model’s confidence predictions to improve global calibration, including Platt scaling [11], temperature scaling [9], histogram binning [12], and

isotonic regression [13]. Platt scaling fits a logistic regression model to a classifier’s scores. Temperature scaling scales the output logits of a neural network by a temperature T trained on the validation set. The adjusted logit values are then put through the softmax function to obtain more calibrated probabilities. Histogram binning partitions confidence scores into bins $\{[0, \epsilon), [\epsilon, 2\epsilon), \dots, [1 - \epsilon, 1]\}$ and sorts each validation sample into a bin based on its confidence $\hat{p}(x)$; it then resets the confidence level of all samples in the bin to match the classification accuracy of that bin. Isotonic regression methods learn a piecewise-constant function on top of the softmax output layer that is trained to fit the output confidence scores to the empirical probabilities in each bin.

2.3 Local Calibration

Two notions of calibration that address some of the deficits of global calibration are class-wise calibration and group-wise calibration. Class-wise calibration groups samples by their true class label [14] and measures the average class ECE, while group-wise calibration uses pre-specified groupings (e.g. race or gender) [15, 16] and measures the average or max ECE over each group. However, in both class-wise and group-wise calibration, the groupings must be known a priori. Additionally, the size of the local neighborhood cannot be varied under these notions of calibration.

A few recalibration methods have been proposed for these notions of calibration as well. However, Dirichlet calibration [14] — a class-wise recalibration method — does not ensure calibration for groupings not based on the label of an example; and while multi-calibration [16] — a group-wise recalibration method — does ensure calibration for a large parametric set of groups, there is no known tractable algorithm to achieve it. [17] introduce a different localized recalibration method, local temperature scaling, an extension of temperature scaling that learns a temperature function $T(x)$, rather than a scalar T ; however, their approach is very specific to semantic segmentation.

At an even more local level, [18] look at individual calibration and conclude that individual calibration is impossible to verify with a deterministic forecaster and thus, there is no general method to train a classifier to achieve individual calibration.

2.4 Kernel-Based Calibration Metrics

[19] introduce the maximum mean calibration error, a kernel-based quantity that replaces the hard binning of the standard ECE estimator with a kernel similarity $k(\hat{p}(x), \hat{p}(x'))$ between the confidence of two examples.

[20] extend their work and propose the more general kernel calibration error.

3 The Local Calibration Error

In this section, we introduce the local calibration error (LCE), a kernel-based metric that allows us to measure the calibration locally around a prediction. Our metric leverages learned features to automatically group similar samples into the same neighborhood, and allows the neighborhood size to be set with a hyperparameter. We mention a few design choices, and then create LCE maps over a 2D feature space, showing that we can use our metric to find areas of local miscalibration.

3.1 Local Calibration Error Metric

We propose a metric to measure calibration locally around a given prediction. The calibration of similar samples should be similar, so we use a kernel similarity function $k(x, x')$, which provides similarity scores, to define local neighborhoods. $k(x, x')$ has bandwidth $\gamma > 0$, which determines the size of the local neighborhood. As γ increases, the neighborhood grows, and the kernel weights the similarity scores such that a sample that is further away in the feature space will have a lower weight.

Let $k_\gamma : \mathcal{X} \times \mathcal{X} \rightarrow \mathbb{R}_+$ be a kernel similarity function with bandwidth $\gamma > 0$ and associated feature map ϕ . Let $a_f(x, y) = \mathbb{1}[f(x) = y]$ indicate whether classifier f makes a correct prediction for input x . Then the signed local calibration error (SLCE) is defined as

$$\text{SLCE}_\gamma(x; f, \hat{p}) := \frac{\mathbb{E}[(\hat{p}(X) - a_f(X, Y))k_\gamma(X, x) \mid \hat{p}(X) = \hat{p}(x)]}{\mathbb{E}[k_\gamma(X, x) \mid \hat{p}(X) = \hat{p}(x)]} \quad (3)$$

and the local calibration error (LCE) is defined as

$$\text{LCE}_\gamma(x; f, \hat{p}) := |\text{SLCE}_\gamma|. \quad (4)$$

Intuitively, this equation considers the neighborhood about a sample x (as defined by the kernel k_γ), and computes the kernel-weighted average of the difference between the confidence and accuracy for each sample in the same confidence bin as x . Note that the LCE has the property that by changing the bandwidth γ , we can interpolate between an individualized calibration metric (as $\gamma \rightarrow 0$) and a global one (as $\gamma \rightarrow \infty$). Lemmas 1 and 2 make this more concrete under the assumption that $\lim_{\gamma \rightarrow 0} k_\gamma(x, x') = \mathbb{1}[x = x']$ and $\lim_{\gamma \rightarrow \infty} k_\gamma(x, x') = 1$. For example, the Laplacian and Gaussian kernels satisfy these conditions.

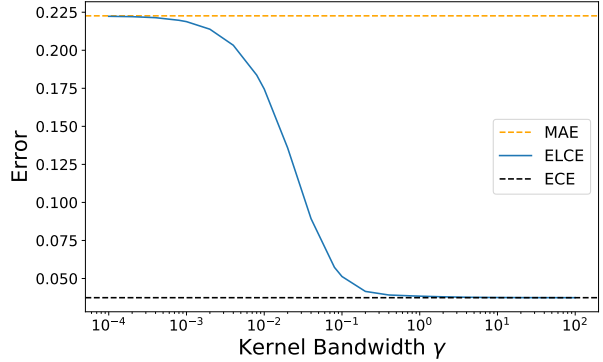


Figure 1: The expected LCE (ELCE) approaches the mean absolute error as $\gamma \rightarrow 0$ and the ECE as $\gamma \rightarrow \infty$. Here, we use a Laplacian kernel with the feature map $\phi_2 \circ \phi_1$, where $\phi_1 : \mathcal{X} \rightarrow \mathbb{R}^{2048}$ is the Inception-v3 model’s hidden layer, and $\phi_2 : \mathbb{R}^{2048} \rightarrow \mathbb{R}^2$ is a t-SNE dimension reduction of these features. We evaluate the LCE of a ResNet-50 classifier on the ImageNet test split.

Lemma 1. *As $\gamma \rightarrow 0$, the expected LCE recovers the L_1 distance between the confidence \hat{p} and accuracy a_f ,*

$$\lim_{\gamma \rightarrow 0} \mathbb{E}[\text{LCE}_\gamma(X; f, \hat{p})] = \mathbb{E}[|\hat{p}(X) - a_f(X, Y)|]$$

Proof. Because $\hat{p}(X)$ and $a_f(X, Y)$ are bounded random variables, that $\lim_{\gamma \rightarrow 0} k_\gamma(x, x') = \mathbb{1}[\phi(x) = \phi(x')]$. For any injective $\phi : \mathcal{X} \rightarrow \mathbb{R}^d$, we have $\mathbb{1}[\phi(x) = \phi(x')] = \mathbb{1}[x = x']$ for all x, x' . This implies the desired result. \square

Lemma 2. *As $\gamma \rightarrow \infty$, the expected LCE recovers the ECE,*

$$\lim_{\gamma \rightarrow \infty} \mathbb{E}[\text{LCE}_\gamma(X; f, \hat{p})] = \text{ECE}(f, \hat{p})$$

Proof. The result follows immediately from observing that $\lim_{\gamma \rightarrow \infty} k_\gamma(x, x') = 1$ for all $x, x' \in \mathcal{X}$. \square

In other words, the expected LCE (ELCE) converges to the mean absolute error (MAE) when γ is small (i.e. the effective neighborhood is very small), and the ECE when γ is large (i.e. the effective neighborhood is very large). Figures 1 and 2 show this phenomenon clearly for a ResNet-50 classifier trained on the ImageNet dataset, each with a different kernel.

As in the ECE calculation, we estimate $\text{LCE}_\gamma(x; f, \hat{p})$ using a binned finite-sample estimator; i.e. we consider sample means over a recalibration set, and we replace the condition $\hat{p}(X) = \hat{p}(x)$ with $B(\hat{p}(X)) = B(\hat{p}(x))$, where $B : [0, 1] \rightarrow \{1, \dots, d\}$ maps a confidence value c to a bin. Detailed formulas for the binned versions as well as a sample complexity analysis of estimating the LCE can be found in Appendix A.

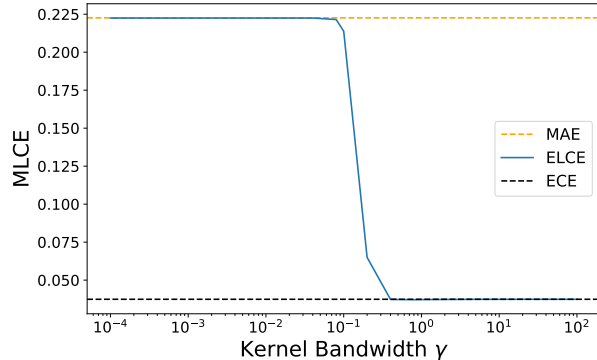


Figure 2: The ELCE transitions much more rapidly between limiting behaviors when the feature map is high-dimensional. Here, we use a Laplacian kernel whose feature map $\phi_1 : \mathcal{X} \rightarrow \mathbb{R}^{2048}$ is the Inception-v3 model’s hidden layer. We evaluate the LCE of a ResNet-50 classifier on the ImageNet test split.

3.2 Choice of Kernel and Feature Map

In this work, we use the Laplacian kernel

$$k_\gamma(x, x') = \exp\left(-\frac{\|\phi(x) - \phi(x')\|_1}{d\gamma}\right)$$

for a pre-defined representation function $\phi : \mathcal{X} \rightarrow \mathbb{R}^d$.

To map an input x to its representation in \mathbb{R}^d , we use a neural network as a feature map ϕ . Features learned from neural networks have proven useful for a wide range of tasks in computer vision, natural language processing, and other areas, and they have been shown to capture useful semantic features of their inputs [21, 22, 23]. The kernel similarity term $k_\gamma(x, x')$ in the LCE is thus able to leverage learned features to *automatically* capture rich subgroups of the data. We chose an Inception-v3 model as our feature map, since Inception features are widely accepted as useful and representative in many areas of machine learning (e.g. for generative models).

In general, we also t-SNE to reduce the dimension of the Inception feature space to e.g. 2 or 3. We find that when using the 2048-dimensional Inception-v3 embedding directly, the ELCE is very sensitive to γ as it transitions rapidly between the limiting behaviors of ELCE as $\gamma \rightarrow 0$ and $\gamma \rightarrow \infty$. One example of this is shown in Figure 2. This effect is likely due to the concentration of $\|\phi(x) - \phi(x')\|$ in high dimension. Reducing the feature dimension with t-SNE greatly reduces the concentration effects observed in Figure 2. The transition between the limiting behaviors is much more gradual, as shown in Figure 1. Thus the overall representation function is $\phi(x) = \phi_2(\phi_1(x))$, where ϕ_1 maps from the inputs to the Inception features, and ϕ_2 reduces the dimensionality of the feature space.

3.3 Local Calibration Error Visualizations

To provide more intuition for the LCE, we will now visualize some examples of the LCE metric over a two-dimensional feature embedding. We consider a ResNet-18 model pre-trained on ImageNet as our classifier (f, \hat{p}) , and the hidden layer representation of an Inception-v3 model pre-trained on ImageNet as a feature map $\phi_1 : \mathcal{X} \rightarrow \mathbb{R}^{2048}$. We then reduce the 2048-dimensional feature vectors with t-SNE to two dimensions for ease of visualization in the LCE landscapes below: $\phi_2 : \mathbb{R}^{2048} \rightarrow \mathbb{R}^2$, so our overall representation function $\phi = \phi_2(\phi_1(x))$. Figure 3 visualizes the landscape of $\text{LCE}_{0.2}(x; f, \hat{p})$ as a function of $\phi(x)$ for the entire ImageNet validation set, as well as the marginal CDF of $\text{LCE}_{0.2}(x, f, \hat{p})$. We show these visualizations for the two confidence bins with the best and worst *global* calibration.

In the bin with the best global calibration, Figure 3 (top) shows that the landscape of the LCE is highly non-uniform, and the CDF of the LCE lies almost entirely to the right of the bin’s average calibration error. Numerically, the bin’s average calibration error is 0.0022, while its average LCE is 0.0259. This implies that the regions where the model is underconfident and overconfident are spatially clustered within the bin. Because global calibration metrics average the miscalibration of these regions to zero, they fail to capture this *localized* miscalibration.

Conversely, in the bin with the worst global calibration, Figure 3 (bottom) shows that the landscape of the LCE is more uniform, and the average calibration error of the bin (0.0455) is much closer to its average LCE (0.0515).

4 LCE Recalibration

In this section, we introduce Local Recalibration (LoRe), a parametric, rank-preserving recalibration method that adjusts a model’s output confidences to achieve better local calibration by learning an additional layer on top of the original model. Our method improves the LCE more than existing recalibration methods, and using our method improves performance on both downstream fairness tasks and downstream decision-making tasks.

4.1 Method Description

For a m -way classification task let $g : \mathbb{R}^d \times \mathbb{R}^m \rightarrow \mathbb{R}^m$ be a rank-preserving neural network whose arguments are feature vector $\phi(x)$ and logits z . This means that

$$g_i(\phi(x), z) < g_j(\phi(x), z) \iff z_i < z_j \quad (5)$$

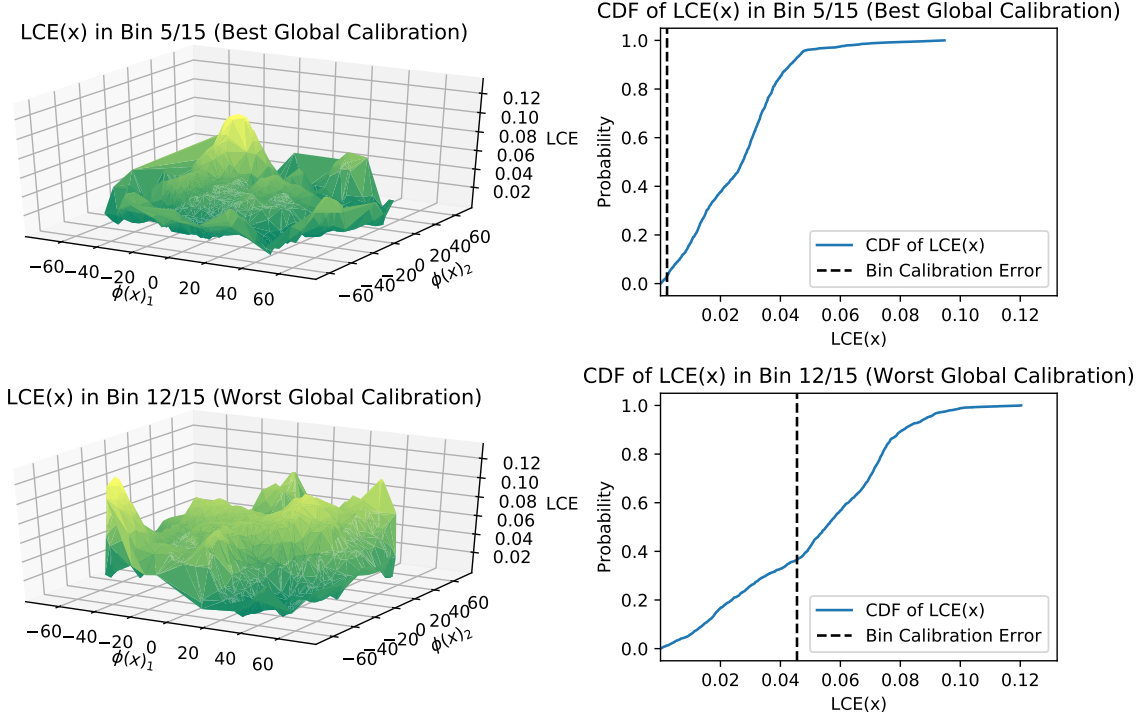


Figure 3: We visualize $LCE_{0.2}(x; f, \hat{p})$ for a ResNet-18 classifier (f, \hat{p}) pre-trained on ImageNet, for every image x in the ImageNet validation set. In the confidence bin with the lowest average calibration error (top), the LCE is highly non-uniform with a large peak. The majority of its CDF lies to the right of the bin’s average calibration error. The LCE thus captures a notion of localized miscalibration that the bin’s average calibration error (used to compute the ECE) misses. In the confidence bin with the worst average calibration error (bottom), there are fewer local patterns in the LCE, so the average calibration error of the bin is more closely aligned with the LCE.

We use a rank-preserving network so our recalibration method leaves the accuracy unchanged. We use a variant of local temperature scaling [17, 24] to parameterize g :

$$t = T^{(\theta_1)}(\phi(x)) \in \mathbb{R}^k \quad (6)$$

$$\tau = (|t| + 1)^{\text{sign}(t)} \in \mathbb{R}^k \quad (7)$$

$$g_\theta(\phi(x), z) = \sum_{i=1}^k \sigma(\tau_i z + B_i^{(\theta_2)}(\phi(x))) \in \mathbb{R}^m \quad (8)$$

Here, $T^{(\theta_1)} : \mathbb{R}^d \rightarrow \mathbb{R}^k$ and $B^{(\theta_2)} : \mathbb{R}^d \rightarrow \mathbb{R}^k$ are neural networks with 1 hidden layer, and σ is a monotone nonlinearity. Equation 7 is a novel formulation for a learned temperature, which we find easier to optimize than alternatives in the literature.

Let \hat{p}' be the recalibrated confidence (i.e. the maximum entry of $z' = \text{softmax}(g(\phi(x), z))$). We train g to return a recalibrated confidence that minimizes the loss $LCE_\gamma(x; f, \hat{p}')$.

In practice, it is challenging to directly optimize the binned estimator for the LCE because the optimization landscape is sensitive to recalibrated probabilities

changing bins. Therefore, we take inspiration from [19] and replace the hard binning with the confidence kernel similarity

$$k_\gamma^n(c, c') = \exp(-n|c - c'|/\gamma) \quad (9)$$

where n is the number of bins used to estimate the LCE.

Within a minibatch $B = \{(x_1, y_1), \dots, (x_b, y_b)\}$, let $c'_i = \hat{p}'(x_i)$ be the recalibrated confidence of x_i , and $a_i = \mathbb{1}[f(x_i) = y_i]$ be the accuracy of f on x_i . We then have the following surrogate loss:

$$L_{\gamma, n}(B) = \frac{1}{b} \cdot \sum_{i=1}^b \left| \frac{\sum_{j=1}^b (c'_j - a_j) k_\gamma(x_i, x_j) k_\gamma^n(c'_i, c'_j)}{\sum_{j=1}^b k_\gamma(x_i, x_j) k_\gamma^n(c'_i, c'_j)} \right| \quad (10)$$

Algorithm 1 provides a practical way to minimize this loss using a gradient-based optimizer like Stochastic Gradient Descent or Adam [25]. We find that good performance on this surrogate loss implies good performance on the binned estimator of the LCE.

Algorithm 1: LoRe

Input: Fixed pre-trained classifier (f, \hat{p}) , fixed feature map ϕ , kernel bandwidth γ , number of bins n .

- 1 Initialize model g // Equations 6, 7, 8
- 2 **foreach** data batch $B = \{(x_1, y_1), \dots, (x_b, y_b)\}$ **do**
- 3 $L \leftarrow L_{\gamma, n}(B)$ // Equation 10
- 4 Update weights of g based on ∇L
- 5 **return** trained model g

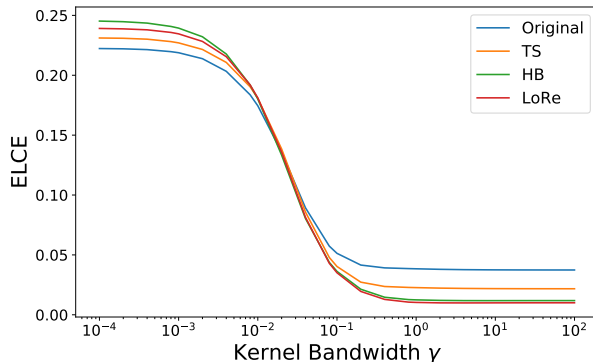


Figure 4: ELCE vs. kernel bandwidth γ for ImageNet. LoRe effectively reduces the ELCE for a wide range of γ , despite only being trained for a single $\gamma = 0.2$.

4.2 Method Performance

Using Algorithm 1, we can substantially improve the LCE values. In Figures 4 and 5, we plot the expected LCE (ELCE) as a function of γ and the maximum LCE (MLCE) as a function of γ , respectively. We can see that our method outperforms both temperature scaling and histogram binning (state of the art global calibration methods) across a wide range of γ values on ImageNet. This is despite the fact that we only train LoRe for a single γ . We show similar results on multiple additional datasets in the next section.

Note that as γ gets large, the ELCE recovers the ECE; because LoRe does well even at large gamma, our method incidentally also works well at minimizing the ECE. Finally, LoRe also lowers the worst-case LCE, suggesting that it leads to lower LCE values across the entire dataset.

5 Experiments

In this section, we run extensive experiments on three datasets to compare our proposed recalibration method against three baselines on fairness and decision-making tasks. We find that our method consistently outperforms the baselines on across a wide

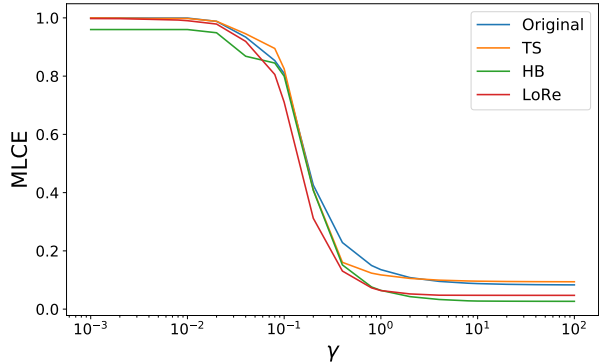


Figure 5: MLCE vs. kernel bandwidth γ for ImageNet. LoRe effectively reduces the MLCE for a wide range of γ . This suggests that LoRe leads to lower LCE values across the whole dataset.

range of γ values, leading to not only better local calibration, but also better performance on both tasks.

We evaluate local calibration through the *maximum* LCE (MLCE). This is because we are interested in understanding a model’s *worst-case* local miscalibration, rather than taking an average like existing global calibration metrics. We show that relative to the baselines, LoRe (with $\gamma = 0.2$) improves the MLCE substantially over a wide range of γ values.

5.1 Datasets

UCI Communities and Crime dataset [26]: This dataset contains a number of attributes about American neighborhoods (e.g. race, age, employment, housing, etc.). The task is to predict the neighborhood’s violent crime rate. The training/validation/test split is 1494 / 500 / 500.

CelebA dataset [27]: A large-scale dataset of face images with 40 attribute annotations (e.g. glasses, hair color, etc.); 202,599 images total. The training/validation/test split is 162,770 / 19,867 / 19,962.

ImageNet dataset [28]: A large-scale dataset of natural scene images with 1000 classes; over 1.3 million images total. The training/validation/test split is 1.3mil / 25,000 / 25,000.

5.2 Downstream Fairness Tasks

5.2.1 Experimental setup

In many fairness-related applications, it is important to show that a model is well-calibrated for all sensitive subgroups of a given population. For example, when predicting the crime rate of a neighborhood, a model should not be considered well-calibrated if it consistently underestimates the crime rate of plurality-white

	1	2	3
No recalibration	0.2089	0.1631	0.1060
Temperature scaling	0.1334	0.0542	0.0764
Histogram binning	0.1319	0.0417	0.0786
LoRe	0.1189	0.0397	0.0650

Table 1: Maximum group-wise ECE (lower is better). Columns indicate the different tasks described in Section 5.2. Rows indicate the type of recalibration method applied. Best results are **bold**.

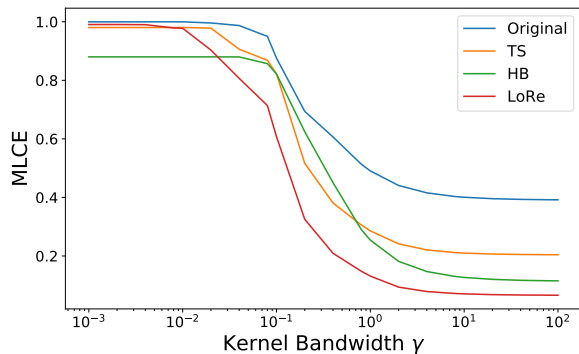


Figure 6: MLCE vs. kernel bandwidth for the UCI Communities and Crime dataset (Task 1 of Section 5.2).

neighborhoods, while overestimating the crime rate of plurality-black neighborhoods.

Therefore, in this section, we examine the group-wise miscalibration of a classifier, as measured by the maximum ECE of a (recalibrated) classifier within any sensitive sub-group. We consider the following experimental settings:

1. UCI Communities and Crime: predict whether a neighborhood’s crime rate is higher than the mean; group neighborhoods by their plurality race (White, Black, Asian, Indian, Hispanic).
2. CelebA: predict a person’s hair color (bald, black, blond, brown, gray, other); group people by hair type (bald, receding hairline, bangs, straight, wavy, other).
3. CelebA: predict a person’s hair type; group people by their hair color; the inverse of setting 2.

For each task, we train classifiers (a simple 3-layer neural network for the UCI crime dataset, and ResNet-50 for CelebA), and recalibrate their output confidences with temperature scaling, histogram binning, and LoRe.

5.2.2 Results

Table 1 reports the maximum group-wise ECE for each of the recalibration methods on each of the three

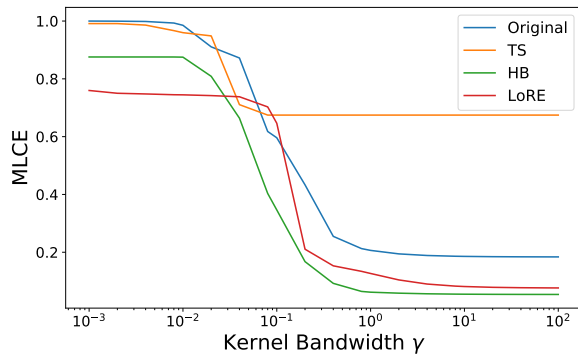


Figure 7: MLCE vs. kernel bandwidth for predicting hair color on CelebA (Task 2 of Section 5.2).

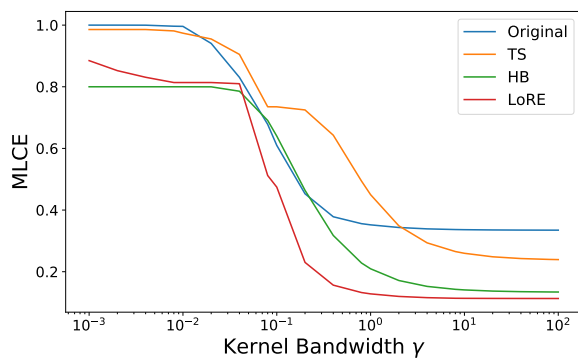


Figure 8: MLCE vs. kernel bandwidth for predicting hair type on CelebA (Task 3 of Section 5.2).

tasks. LoRe clearly outperforms the other three baselines, achieving an average 52% reduction over no recalibration and an average 11% improvement over the next best recalibration method.

In Figures 6, 7, and 8, we show MLCE curves for no recalibration, temperature scaling, histogram binning, and LoRe. For tasks 1 and 3 (Figures 6 and 8), LoRe significantly improves the local calibration. For task 2 (Figure 7, LoRe outperforms temperature scaling on both maximum group-wise ECE and MLCE. Compared to histogram binning, it attains slightly better maximum ECE but slightly worse MLCE. Overall, we can see that the MLCE and maximum groupwise ECE are correlated metrics. More broadly, our results indicate that lowering the LCE has positive implications in fairness settings.

5.3 Downstream Decision-Making Tasks

5.3.1 Experimental Setup

Machine learning predictions are often used to make decisions, and in many situations an agent must select a best action in expectation. As an example, suppose there is a cost $w = -10$ associated with an

	Reward	PRR
No recalibration	-17827	0.5658
Temperature scaling	-17320	0.5615
Histogram binning	-17465	0.4611
LoRe	-17048	0.5747

Table 2: Performance on downstream decision-making. Columns from left to right indicate the total reward (higher is better) and the PRR (higher is better). Rows indicate the type of recalibration applied. Best results **bold**.

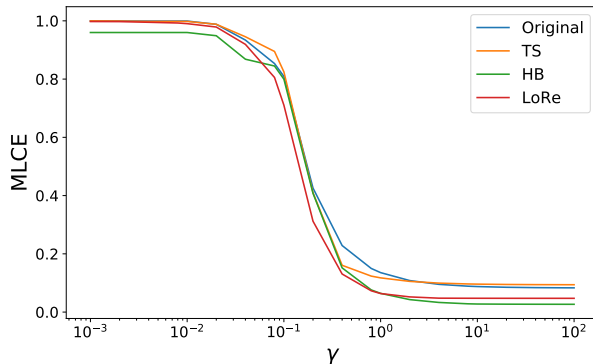


Figure 9: MLCE vs. kernel bandwidth on the ImageNet dataset (lower is better). LoRe outperforms the baselines for γ values between the two extremes.

incorrect classification and a cost $u = -1$ associated with “unsure” (e.g. in situations such as autonomous driving, making an incorrect classification incurs a high cost but being unsure incurs only the small cost of calling a human operator). An agent with good uncertainty quantification can make a more optimal decision about whether to return a classification or return “unsure”; for a calibrated model, the agent will return “unsure” below the confidence threshold of $1 - (1/(w + u))$, and return a prediction above it.

We train a ResNet-50 model on ImageNet and recalibrate the output confidences with temperature scaling, histogram binning, and LoRe. The resulting MLCE values are plotted for no recalibration, temperature scaling, histogram binning, and LoRe. We then calculate the total reward (given the above cost function) as well as the prediction rejection area ratio (PRR) [29], which measures the quality of the rejection curve when a model can choose to not provide any prediction, for each of these four methods. Note that a PRR of 1.0 indicates optimal rejection, and a PRR of 0.0 indicates “random” rejection; a higher PRR is better.

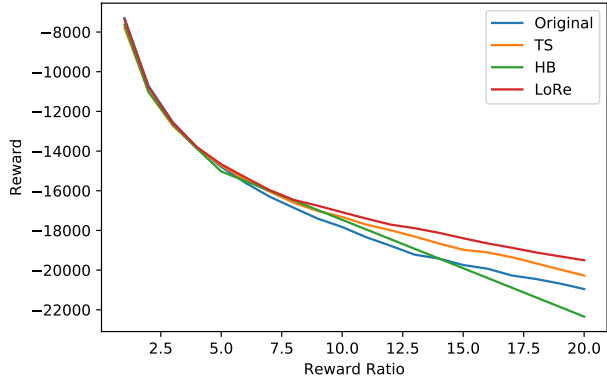


Figure 10: Reward attained vs. reward ratio for the ImageNet dataset (higher is better). LoRe achieves the highest rewards.

5.3.2 Results

Table 2 reports the reward and PRR achieved with each method given the cost function described above; LoRe clearly outperforms the other three baselines. In Figure 9, we show the MLCE curves for no recalibration, temperature scaling, histogram binning, and LoRe; LoRe again outperforms the other three baselines for γ values between the two extremes (i.e. for medium-sized neighborhoods). In addition, in Figure 10, we show the total reward as a function of the reward ratio (i.e. the cost of an incorrect classification to the cost of being unsure). Across a wide range of reward ratios, LoRe still achieves the highest reward. These results indicate that our recalibration method most effectively lowers LCE values, and that these lower LCE values correspond to better performance on this decision-making task.

6 Conclusion

In this paper, we introduced the local calibration error, a metric that measures calibration in a localized neighborhood around a prediction. The LCE spans the gap between fully global and fully individualized calibration error, with an effective neighborhood size that can be set with a bandwidth parameter γ . We also introduced LoRe, a recalibration method that greatly improves the local calibration. Finally, we demonstrated that achieving lower LCE values leads to better performance on downstream fairness or decision-making tasks. In future work, we are interested in investigating more localized forms of different notions of uncertainty quantification.

References

- [1] A. Kendall and Y. Gal, “What uncertainties do we need in bayesian deep learning for computer vision?,” in *Advances in neural information processing systems*, pp. 5574–5584, 2017.
- [2] L. Yang, X. Liang, T. Wang, and E. P. Xing, “Real-to-virtual domain unification for end-to-end autonomous driving,” in *ECCV*, 2018.
- [3] H. Berestycki, J. Busca, and I. Florent, “Asymptotics and calibration of local volatility models,” *Quantitative finance*, vol. 2, no. 1, pp. 61–69, 2002.
- [4] J. Khan, J. S. Wei, M. Ringner, L. H. Saal, M. Ladanyi, F. Westermann, F. Berthold, M. Schwab, C. R. Antonescu, C. Peterson, *et al.*, “Classification and diagnostic prediction of cancers using gene expression profiling and artificial neural networks,” *Nature medicine*, vol. 7, no. 6, p. 673, 2001.
- [5] W. Chen, B. Sahiner, F. W. Samuelson, A. Pezeshk, and N. A. Petrick, “Calibration of medical diagnostic classifier scores to the probability of disease,” *Statistical methods in medical research*, vol. 27, pp. 1394 – 1409, 2018.
- [6] G. W. Brier, “Verification of forecasts expressed in terms of probability,” *Monthly weather review*, vol. 78, no. 1, pp. 1–3, 1950.
- [7] T. Gneiting, F. Balabdaoui, and A. E. Raftery, “Probabilistic forecasts, calibration and sharpness,” *Journal of the Royal Statistical Society: Series B (Statistical Methodology)*, vol. 69, no. 2, pp. 243–268, 2007.
- [8] N. Cesa-Bianchi and G. Lugosi, *Prediction, learning, and games*. Cambridge university press, 2006.
- [9] C. Guo, G. Pleiss, Y. Sun, and K. Q. Weinberger, “On calibration of modern neural networks,” in *Proceedings of the 34th International Conference on Machine Learning* (D. Precup and Y. W. Teh, eds.), vol. 70 of *Proceedings of Machine Learning Research*, (International Convention Centre, Sydney, Australia), pp. 1321–1330, PMLR, 06–11 Aug 2017.
- [10] M. P. Naeini, G. F. Cooper, and M. Hauskrecht, “Obtaining well calibrated probabilities using bayesian binning,” in *AAAI*, p. 2901–2907, 2015.
- [11] J. C. Platt, “Probabilistic outputs for support vector machines and comparisons to regularized likelihood methods,” in *Advances in Large Margin Classifiers*, pp. 61–74, MIT Press, 1999.
- [12] B. Zadrozny and C. Elkan, “Obtaining calibrated probability estimates from decision trees and naive bayesian classifiers,” in *In Proceedings of the Eighth International Conference on Machine Learning*, pp. 609–616, Morgan Kaufmann, 2001.
- [13] B. Zadrozny and C. Elkan, “Transforming classifier scores into accurate multiclass probability estimates,” in *SIGKDD*, 2002.
- [14] M. Kull, M. Perello Nieto, M. Kängsepp, T. Silva Filho, H. Song, and P. Flach, “Beyond temperature scaling: Obtaining well-calibrated multi-class probabilities with dirichlet calibration,” in *Advances in Neural Information Processing Systems* (H. Wallach, H. Larochelle, A. Beygelzimer, F. d’Alché-Buc, E. Fox, and R. Garnett, eds.), vol. 32, pp. 12316–12326, Curran Associates, Inc., 2019.
- [15] J. M. Kleinberg, S. Mullainathan, and M. Raghavan, “Inherent trade-offs in the fair determination of risk scores,” 2016.
- [16] Ú. Hébert-Johnson, M. P. Kim, O. Reingold, and G. N. Rothblum, “Calibration for the (computationally-identifiable) masses,” 2017.
- [17] Z. Ding, X. Han, P. Liu, and M. Niethammer, “Local temperature scaling for probability calibration,” 2020.
- [18] S. Zhao, T. Ma, and S. Ermon, “Individual calibration with randomized forecasting,” in *ICML*, 2020.
- [19] A. Kumar, S. Sarawagi, and U. Jain, “Trainable calibration measures for neural networks from kernel mean embeddings,” in *Proceedings of the 35th International Conference on Machine Learning* (J. Dy and A. Krause, eds.), vol. 80 of *Proceedings of Machine Learning Research*, (Stockholmsmässan, Stockholm Sweden), pp. 2805–2814, PMLR, 10–15 Jul 2018.
- [20] D. Widmann, F. Lindsten, and D. Zachariah, “Calibration tests in multi-class classification: A unifying framework,” in *Advances in Neural Information Processing Systems* (H. Wallach, H. Larochelle, A. Beygelzimer, F. d’Alché-Buc, E. Fox, and R. Garnett, eds.), vol. 32, Curran Associates, Inc., 2019.
- [21] M. Huh, P. Agrawal, and A. A. Efros, “What makes imagenet good for transfer learning?,” 2016.
- [22] T. Chen, S. Kornblith, M. Norouzi, and G. Hinton, “A simple framework for contrastive learning of visual representations,” in *Proceedings of the 37th International Conference on Machine Learning* (H. D. III and A. Singh, eds.), vol. 119 of *Proceedings of Machine Learning Research*, pp. 1597–1607, PMLR, 13–18 Jul 2020.
- [23] B. Li, H. Zhou, J. He, M. Wang, Y. Yang, and L. Li, “On the sentence embeddings from pre-trained language models,” in *Proceedings of the 2020 Conference on Empirical Methods in Natural Language Processing (EMNLP)*, pp. 9119–9130, Association for Computational Linguistics, Nov. 2020.
- [24] Y. Bai, T. Ma, H. Wang, and C. Xiong, “Improved uncertainty post-calibration via rank preserving transforms,” 2021.

- [25] D. P. Kingma and J. Ba, “Adam: A method for stochastic optimization,” in *ICLR*, 2015.
- [26] D. Dua and C. Graff, “UCI machine learning repository,” 2017.
- [27] Z. Liu, P. Luo, X. Wang, and X. Tang, “Deep learning face attributes in the wild,” in *Proceedings of International Conference on Computer Vision (ICCV)*, December 2015.
- [28] J. Deng, W. Dong, R. Socher, L.-J. Li, K. Li, and L. Fei-Fei, “Imagenet: A large-scale hierarchical image database,” in *2009 IEEE conference on computer vision and pattern recognition*, pp. 248–255, Ieee, 2009.
- [29] A. Malinin, B. Mlodozieniec, and M. Gales, “Ensemble distribution distillation,” *ArXiv*, vol. abs/1905.00076, 2020.

A Analysis of the localized calibration error

We consider binned versions of the SLCE (and LCE) where we replace the exact conditioning by a binned version. Let B_1, \dots, B_N denote a set of bins that partition $[0, 1]$, and $B(p)$ denote the bin $p \in [0, 1]$ belongs to. We consider the binned version of the SLCE:

$$\begin{aligned} \text{SLCE}_\gamma(x; f, \hat{p}) &:= \frac{\mathbb{E}[(\hat{p}(X) - a_f(X, Y))k_\gamma(X, x) \mid \hat{p}(X) \in B(\hat{p}(x))]}{\mathbb{E}[k_\gamma(X, x) \mid \hat{p}(X) \in B(\hat{p}(x))]} \\ &= \frac{\mathbb{E}[(\hat{p}(X) - a_f(X, Y))k_\gamma(X, x)\mathbb{1}[\hat{p}(X) \in B(\hat{p}(x))]]}{\mathbb{E}[k_\gamma(X, x)\mathbb{1}[\hat{p}(X) \in B(\hat{p}(x))]]}. \end{aligned}$$

We make the following assumptions:

Assumption A (Lipschitz kernel). *The kernel k_γ takes the form*

$$k_\gamma(x, x') = f\left(\frac{\phi(x) - \phi(x')}{\gamma}\right),$$

where $\phi : \mathcal{X} \rightarrow \mathbb{R}^d$ is a representation function, and $f : \mathbb{R}^d \rightarrow [0, 1]$ is L -Lipschitz with respect to some norm $\|\cdot\|$.

Note this definition may require an implicit rescaling (for example, we can take $\phi(x) \leftarrow \phi^{\text{feature}}(x)/d$ for a d -dimensional feature map ϕ^{feature} and take $f(z) = \exp(-\|z\|_1)$, which corresponds to the Laplacian kernel we used in Section 3.2).

Assumption B (Binning-aware covering number). *For any $\epsilon > 0$, the range of the representation function $\phi(\mathcal{X}) := \{\phi(x) : x \in \mathcal{X}\}$ has an ϵ -cover in the $\|\cdot\|$ -norm of size $(C/\epsilon)^d$ for some absolute constant $C > 0$: There exists a set $\mathcal{N}_\epsilon \in \mathcal{X}$ with $|\mathcal{N}_\epsilon| \leq (C/\epsilon)^d$ such that for any $x \in \mathcal{X}$, there exists some $x' \in \mathcal{N}_\epsilon$ such that $\|\phi(x) - \phi(x')\| \leq \epsilon$ and $B(\hat{p}(x)) = B(\hat{p}(x'))$.*

Assumption C (Lower bound on expectation of kernel within bin). *We have*

$$\inf_{x \in \mathcal{X}} \mathbb{E}[k_\gamma(X, x)\mathbb{1}[\hat{p}(X) \in B(\hat{p}(x))]] \geq \underline{c}$$

for some constant $\underline{c} \in (0, 1)$.

The constant \underline{c} characterizes the hardness of estimating the SLCE from samples. Intuitively, with a smaller \underline{c} , the denominator in SLCE gets smaller and we desire a higher accuracy in estimating both the numerator and the denominator. Also note that in practice the value of \underline{c} typically depends on γ .

We analyze the following estimator of the SLCE using n samples:

$$\widehat{\text{SLCE}}_\gamma(x; f, \hat{p}) = \frac{\frac{1}{n} \sum_{i=1}^n (\hat{p}(x_i) - a_f(x_i, y_i))k_\gamma(x_i, x)\mathbb{1}[\hat{p}(x_i) \in B(\hat{p}(x))]}{\frac{1}{n} \sum_{i=1}^n k_\gamma(x_i, x)\mathbb{1}[\hat{p}(x_i) \in B(\hat{p}(x))]}. \quad (11)$$

Theorem 1. *Under Assumptions A, B, and C, Suppose the sample size $n \geq \tilde{O}(d/\underline{c}^4\epsilon^2)$ where $\epsilon > 0$ is a target accuracy level, then with probability at least $1 - \delta$ we have*

$$\sup_{x \in \mathcal{X}} \left| \widehat{\text{SLCE}}_\gamma(x; f, \hat{p}) - \text{SLCE}_\gamma(x; f, \hat{p}) \right| \leq \epsilon,$$

where \tilde{O} hides log factors of the form $\log(L/\gamma\epsilon\delta\underline{c})$.

Theorem 1 shows that $\tilde{O}(d/\epsilon^2\underline{c}^4)$ samples is sufficient to estimate the SLCE simultaneously for all $x \in \mathcal{X}$. When $\underline{c} = \Omega(1)$, this sample complexity only depends polynomially in terms of the representation dimension d and logarithmically in other constants (such as L, γ , and the failure probability δ).

A.1 Proof of Theorem 1

Step 1. We first study the estimation at finitely many x 's. Let $\mathcal{N} \subseteq \mathcal{X}$ be a finite set of x 's with $|\mathcal{N}| = N$. Since $k_\gamma \in [0, 1]$ and $|\hat{p}(x) - a_f(x, y)| \leq 1$ are bounded variables, by the Hoeffding inequality and a union bound, we have

$$\begin{aligned} & \mathbb{P}\left(\sup_{x \in \mathcal{N}} \left| \frac{1}{n} \sum_{i=1}^n (\hat{p}(x_i) - a_f(x_i, y_i)) k_\gamma(x_i, x) \mathbb{1}[\hat{p}(x_i) \in B(\hat{p}(x))] \right. \right. \\ & \quad \left. \left. - \mathbb{E}[(\hat{p}(X) - a_f(X, Y)) k_\gamma(X, x) \mathbb{1}[\hat{p}(X) \in B(\hat{p}(x))]] \right| > \underline{c}\epsilon/10\right) \\ & \leq \exp(-cn\underline{c}^2\epsilon^2 + \log N). \end{aligned}$$

Therefore, as long as $n \geq O(\log(N/\delta)/\epsilon^2\underline{c}^2)$ samples, the above probability is bounded by δ . In other words, with probability at least $1 - \delta$, we have simultaneously

$$\left| \underbrace{\frac{1}{n} \sum_{i=1}^n (\hat{p}(x_i) - a_f(x_i, y_i)) k_\gamma(x_i, x) \mathbb{1}[\hat{p}(x_i) \in B(\hat{p}(x))]}_{:=\hat{A}(x)} - \underbrace{\mathbb{E}[(\hat{p}(X) - a_f(X, Y)) k_\gamma(X, x) \mathbb{1}[\hat{p}(X) \in B(\hat{p}(x))]]}_{:=A(x)} \right| \leq \underline{c}\epsilon/10.$$

for all $x \in \mathcal{N}$. Similarly, when $n \geq O(\log(N/\delta)/\epsilon^2\underline{c}^4)$, we also have (with probability at least $1 - \delta$)

$$\left| \underbrace{\frac{1}{n} \sum_{i=1}^n k_\gamma(x_i, x) \mathbb{1}[\hat{p}(x_i) \in B(\hat{p}(x))]}_{:=\hat{B}(x)} - \underbrace{\mathbb{E}[k_\gamma(X, x) \mathbb{1}[\hat{p}(X) \in B(\hat{p}(x))]]}_{:=B(x)} \right| \leq \underline{c}^2\epsilon/10$$

On these concentration events, we have for any $x \in \mathcal{N}$ that

$$\begin{aligned} & \left| \widehat{\text{SLCE}}_\gamma(x; f, \hat{p}) - \text{SLCE}_\gamma(x; f, \hat{p}) \right| = \left| \frac{\hat{A}(x)}{\hat{B}(x)} - \frac{A(x)}{B(x)} \right| \leq \left| \frac{\hat{A}(x)}{\hat{B}(x)} \right| \left| \frac{1}{\hat{B}(x)} - \frac{1}{B(x)} \right| + \frac{1}{|B(x)|} |\hat{A}(x) - A(x)| \\ & \leq 1 \cdot \frac{\underline{c}^2\epsilon/10}{\underline{c}(\underline{c} - \underline{c}^2\epsilon/10)} + \frac{1}{\underline{c}} \cdot \underline{c}\epsilon/10 \leq \epsilon. \end{aligned}$$

Step 2. We now extend the bound to all $x \in \mathcal{X}$ using the covering argument. By Assumption B, we can take an $\underline{c}^2\epsilon\gamma/(10L)$ -covering of $\phi(\mathcal{X})$ with cardinality $N \leq (10CL/\underline{c}^2\epsilon\gamma)^d$. Let $\mathcal{N} \subset \mathcal{X}$ denote the covering set (in the \mathcal{X} space). This means that for any $x \in \mathcal{X}$, there exists $x' \in \mathcal{N}$ such that $\|\phi(x) - \phi(x')\| \leq \underline{c}^2\epsilon\gamma/(10L)$ and $B(\hat{p}(x)) = B(\hat{p}(x'))$, which implies that for any $\tilde{x} \in \mathcal{X}$ we have

$$\begin{aligned} & |k(\tilde{x}, x) - k(\tilde{x}, x')| = \left| f\left(\frac{\phi(\tilde{x}) - \phi(x)}{\gamma}\right) - f\left(\frac{\phi(\tilde{x}) - \phi(x')}{\gamma}\right) \right| \\ & \leq \frac{L}{\gamma} \|\phi(x) - \phi(x')\| \leq \underline{c}^2\epsilon/10, \end{aligned}$$

where we have used the Lipschitzness assumption of f (Assumption A). This further implies

$$\begin{aligned} & \left| \hat{A}(x) - \hat{A}(x') \right| \\ & = \left| \frac{1}{n} \sum_{i=1}^n (\hat{p}(x_i) - a_f(x_i, y_i)) k_\gamma(x_i, x) \mathbb{1}[\hat{p}(x_i) \in B(\hat{p}(x))] - \frac{1}{n} \sum_{i=1}^n (\hat{p}(x_i) - a_f(x_i, y_i)) k_\gamma(x_i, x') \mathbb{1}[\hat{p}(x_i) \in B(\hat{p}(x'))] \right| \\ & = \left| \frac{1}{n} \sum_{i=1}^n (\hat{p}(x_i) - a_f(x_i, y_i)) [k_\gamma(x_i, x) - k_\gamma(x_i, x')] \mathbb{1}[\hat{p}(x_i) \in B(\hat{p}(x))] \right| \\ & \leq \frac{1}{n} \sum_{i=1}^n |\hat{p}(x_i) - a_f(x_i, y_i)| \cdot |k_\gamma(x_i, x) - k_\gamma(x_i, x')| \mathbb{1}[\hat{p}(x_i) \in B(\hat{p}(x))] \leq \underline{c}^2\epsilon/10. \end{aligned}$$

Similarly, we have $|A(x) - A(x')| \leq \underline{c}^2\epsilon/10$, $|\hat{B}(x) - \hat{B}(x')| \leq \underline{c}^2\epsilon/10$, and $|B(x) - B(x')| \leq \underline{c}^2\epsilon/10$. This means that the estimation error at x is close to that at $x' \in \mathcal{N}$ and consequently also bounded by ϵ :

$$\begin{aligned} & \left| \widehat{\text{SLCE}}_\gamma(x; f, \hat{p}) - \text{SLCE}_\gamma(x; f, \hat{p}) \right| = \left| \frac{\hat{A}(x)}{\hat{B}(x)} - \frac{A(x)}{B(x)} \right| \\ & \leq \left| \frac{\hat{A}(x)}{\hat{B}(x)} - \frac{\hat{A}(x')}{\hat{B}(x')} \right| + \left| \frac{\hat{A}(x')}{\hat{B}(x')} - \frac{A(x')}{B(x')} \right| + \left| \frac{A(x')}{B(x')} - \frac{A(x)}{B(x)} \right| \\ & \leq 3 \left[1 \cdot \frac{\underline{c}^2\epsilon/10}{\underline{c}(\underline{c} - \underline{c}^2\epsilon/10)} + \frac{1}{\underline{c}} \cdot \underline{c}^2\epsilon/10 \right] \leq \epsilon. \end{aligned}$$

Therefore, taking this \mathcal{N} in step 1, we know that as long as the sample size

$$N \geq O\left(\frac{\log(|\mathcal{N}|/\delta)}{\epsilon^2 \underline{c}^4}\right) = O\left(\frac{d[\log(10CL/\underline{c}^2\epsilon\gamma) + \log(1/\delta)]}{\underline{c}^4\epsilon^2}\right) = \tilde{O}(d/\underline{c}^4\epsilon^2),$$

we have with probability at least $1 - \delta$ that

$$\sup_{x \in \mathcal{X}} \left| \widehat{\text{SLCE}}_\gamma(x; f, \hat{p}) - \text{SLCE}_\gamma(x; f, \hat{p}) \right| \leq \epsilon.$$

This is the desired result. □